ADA035970

SQUARE WAVE VOLTAMMETRY
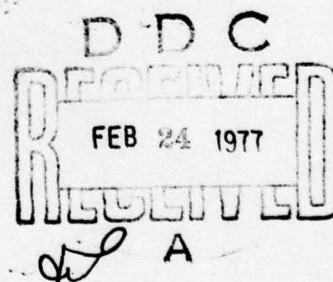
AT THE DROPPING MERCURY

ELECTRODE: THEORETICAL

by

J. H. Christie, John A. Turner and R. A. Osteryoung

Colorado State University
Department of Chemistry
Fort Collins, Colorado 80523

February, 1977

DDC

FEB 24 1977

RECEIVED

A

REPORT DOCUMENTATION PAGE		READ INSTRUCTIONS BEFORE COMPLETING FORM
1. REPORT NUMBER Technical Report No. 2	2. GOVT ACCESSION NO.	3. RECIPIENT'S CATALOG NUMBER
4. TITLE (and Subtitle) Square Wave Voltammetry at the Dropping Mercury Electrode: Theoretical.		5. TYPE OF REPORT & PERIOD COVERED Interim
		6. PERFORMING ORG. REPORT NUMBER
7. AUTHOR(s) J. H. Christie, John A. Turner and R. A. Osteryoung		8. CONTRACT OR GRANT NUMBER(s) N00014-77-C-004
9. PERFORMING ORGANIZATION NAME AND ADDRESS Department of Chemistry Colorado State University Fort Collins, Colorado 80523		10. PROGRAM ELEMENT, PROJECT, TASK AREA & WORK UNIT NUMBERS
11. CONTROLLING OFFICE NAME AND ADDRESS Chemistry Program Office of Naval Research Arlington, Virginia 22217		12. REPORT DATE Feb 1977
		13. NUMBER OF PAGES 24
14. MONITORING AGENCY NAME & ADDRESS(if different from Controlling Office) Office of Naval Research Resident Representative Suite 210, 6740 E. Hampden Avenue Denver, Colorado 80222	26p.	15. SECURITY CLASS. (of this report) Unclassified
		15a. DECLASSIFICATION/DOWNGRADING SCHEDULE

16. DISTRIBUTION STATEMENT (of this Report)

Approved for Public Release; Distribution Unlimited

TR-2   N00014-77-C-0004

17. DISTRIBUTION STATEMENT (of the abstract entered in Block 20, if different from Report)

18. SUPPLEMENTARY NOTES

19. KEY WORDS (Continue on reverse side if necessary and identify by block number)

square wave voltammetry; dropping mercury electrode; electroanalytical chemistry.

20. ABSTRACT (Continue on reverse side if necessary and identify by block number)

The theoretical aspects of square wave voltammetry at the dropping mercury electrode are presented. The technique involves scanning the entire potential range of interest on a single drop of a dme. Asymmetries in the waveform as well as variations in current measurement parameters are discussed. Indications are that previous uses of the waveform may not have utilized all its capabilities.

DD $_{1\text{ JAN }73}^{\text{FORM}}$ 1473   EDITION OF 1 NOV 65 IS OBSOLETE
S/N 0102-014-6601

404 992

BRIEF

The theoretical response for the application of square wave voltammetry at a dropping mercury electrode is presented, with particular reference to points of current measurement.

ABSTRACT

The theoretical aspects of square wave voltammetry at the dropping mercury electrode are presented. The technique involves scanning the entire potential range of interest on a single drop of a dme. Asymmetries in the waveform as well as variations in current measurement parameters are discussed. Indications are that previous uses of the waveform may not have utilized all its capabilities.

For the past several years, we have been concerned with development and application of pulse polarography and voltammetry (1). The advantages of these pulse techniques reside chiefly in their discrimination against double layer charging currents, but, as they are usually applied, they are relatively slow: only one measurement is made per drop of the dme and a ratio of delay time to pulse time of 10:1 or greater is normally employed.

Recently a modification to the PAR 174 was introduced (2) which allows it to do a fast sweep mode of differential pulse polarography. One of the problems inherent with this modification arises from the linear ramp used as the base potential sweeping function. The required high slope of the linear ramp reintroduces charging current background that the differential pulse technique was intended to discriminate against. This fast sweep technique also suffers from resolution problems at sweep rates greater than 200 mV/sec in that insufficient points are taken to define the peaks.

We now turn to the technique of square wave voltammetry at the dme which retains a high discrimination against double layer charging current but which allows measurement of a complete potential range during the life of a single drop at the dme. This technique was reported by Barker (3) as long ago as 1957, but has since seen little application. Ramaley and Krause have developed the theory (4) and have presented some application (5) of square wave voltammetry at the hanging mercury drop electrode.

The discussions of Ramaley and Krause were limited to small step heights (and consequent slow scan rates). In order to carry out experiments within the life of a single drop of a DME, faster scan rates (>100 mV/sec) are required. Faster scan rates imply relatively larger step heights for the underlying staircase wave-form. While the equations presented below are valid for all values of experimental parameters, our calculations concentrate on those values which are useful in our particular case.

Our fundamental potential wave-form differs superficially from that of Ramaley and Krause in that the phase of the square wave is shifted by π relative to the staircase. Our treatment also includes the possibility of some asymmetries in wave-form and measurement times not considered by Ramaley and Krause.

We develop our treatment for a stationary planar electrode; it is shown in a later paper (6) that the effects of drop growth can be well compensated by an area normalization of the observed currents.

The general square wave-form, shown in Figure 1, can be thought of as a pair of pulses superimposed on a staircase wave-form. One of the pulses is coincident with the step advance of the staircase, while the other is in the opposite sense and lasts until the end of the potential step. In the work of Ramaley (4,5), the first pulse is opposite in sense to the staircase direction while in our case the pulse coincident with staircase advance is in the ascending staircase scan direction. In the work presented here, the two pulses are of equal amplitude (with respect to the basic staircase) but need not be of equal duration.

The nomenclature we use is adapted from that of staircase voltammetry (7) and differs somewhat from that of Barker (8) and Ramaley (4,5). The basic time unit, τ, corresponds to the step width in staircase voltammetry and ΔE is the step height. For the square wave-form, some additional parameters must be introduced as shown in Figure 1. The square wave amplitude is E_{sw} and corresponds to the magnitude of each of the two potential pulses (with respect to the staircase potential). The fraction of each period during which the potential is "up" is σ; the length of the forward pulse therefore is $\sigma\tau$. The current is measured twice during each staircase period: at time $\rho_1\tau$ during the forward pulse and at time $\rho_2\tau$ during the reverse pulse. The coefficient ρ_1, ρ_2, and σ are all fractions less than unity and

$\rho_1 < \sigma < \rho_2$. The treatment of Ramaley and Krause was restricted to the symmetric case in which $\sigma = 0.5$ and $\rho_1 = \rho_2 - \sigma$. The usual output is the difference in current measurement at $\rho_1 \tau$ and $\rho_2 \tau$ during the same staircase period, which we call the forward difference and designate ΔI^+, but other differencing schemes are possible.

Assuming semi-infinite linear diffusion and a reversible electrode reaction with only the oxidized form initially present in solution, the equation for the currents can be obtained by straight-forward application of the superposition theorem (9) or by generalization and modification of the arbitrary wave-form equation presented by Rifkin and Evans (10).

During the jth period of the staircase, the current measured at $\rho_1 \tau$ during the forward pulse is

$$I_f(j) = \frac{nFAD_0^{\frac{1}{2}}}{\sqrt{\pi\tau}} \left\{ \frac{C_2(j-1)-C_1(j)}{\rho_1^{\frac{1}{2}}} + \sum_{m=0}^{j-1} \frac{C_2(m-1)-C_1(m)}{(j-m+\rho_1)^{\frac{1}{2}}} + \frac{C_1(m)-C_2(m)}{(j-m+\rho_1-\sigma)^{\frac{1}{2}}} \right\} \quad (1)$$

and the current at $\rho_2 \tau$ during the reverse pulse is

$$I_r(j) = \frac{nFAD_0^{\frac{1}{2}}}{\sqrt{\pi\tau}} \sum_{m=0}^{j} \left\{ \frac{C_2(m-1)-C_1(m)}{(j-m+\rho_2)^{\frac{1}{2}}} + \frac{C_1(m)-C_2(m)}{(j-m+\rho_2-\sigma)^{\frac{1}{2}}} \right\} \quad (2)$$

In Equations (1) and (2), the terms of the type $C_1(k)$ are the surface concentration of oxidant during the forward pulse of the kth period. Terms of the form $C_2(k-1)$ and $C_2(k)$ are the surface concentrations during the reverse pulses of the (k-1) and kth periods, respectively. Numbering of the periods starts with j=o and $C_2(-1)$ (for the first period) is the bulk concentration C*.

For a planar electrode and a simple reversible reaction, the surface concentration of oxidant is fixed by the potential

$$C_0(0,t) = \frac{C*}{1+\epsilon(t)} \quad (3)$$

where

$$\varepsilon(t) = \exp\left\{-\frac{nF}{RT}\left[E(t)-E_{\frac{1}{2}}^{r}\right]\right\} \tag{4}$$

and $E_{\frac{1}{2}}^{r}$ is the reversible half wave potential.

Combining the potential wave-forms:

$$E_1(k) = E_i - k\Delta E - E_{sw} \tag{5}$$

during the forward pulse and

$$E_2(k) = E_i - k\Delta E + E_{sw} \tag{6}$$

during the reverse pulse with Equation (3) giving the explicit surface con-
centration to be used in Equations (1) and (2).

The forward current can then be written

$$I_f(j) = \frac{nFAD_0^{\frac{1}{2}}C*}{\sqrt{\pi\tau}} \ \psi_f \ (E_{sw}, \ \Delta E, \ \rho_1, \ \sigma) \tag{7}$$

and the reverse current

$$I_r(j) = \frac{nFAD_0^{\frac{1}{2}}C*}{\sqrt{\pi\tau}} \ \psi_r \ (E_{sw}, \ \Delta E, \ \rho_2, \ \sigma) \tag{8}$$

The forward difference current is

$$\Delta I^+(j) = I_f(j) - I_r(j) = \frac{nFAD_0^{\frac{1}{2}}C*}{\sqrt{\pi\tau}}\left(\psi_f(j)-\psi_r(j)\right) = \frac{nFAD_0^{\frac{1}{2}}C*}{\sqrt{\pi\tau}} \Delta\psi^+(j) \tag{9}$$

The explicit formulation of the ψ functions can be written by combining
Equations (5) and (6) with Equations (3) and (4) and substituting the results
into Equations (1) and (2).

Theoretical square wave voltammograms were generated for a variety of
experimental parameters. The computer program explicitly calculates and
stores the component forward and reverse current functions ψ_f and ψ_r rather
than merely the difference function $\Delta\psi^+$. Consideration of the partial cur-
rents greatly facilitates the understanding of the results. The program
was written in Fortran IV and was run on Digital Equipment Corp. PDP-12
computer.

Calculated square wave current-potential functions for several values of E_{sw} are shown in Figure 2. The difference current is always an essentially symmetric peak shaped function, but for small square wave amplitude is smaller than either the forward or reverse currents (Figure 2A). The effect of square wave amplitude on the component currents and on the difference current is clearly shown in Figure 3. Only for $n\,E_{sw} > \sim 15$ mV does the reverse current in the vicinity of the half-wave potential become negative and the difference current become larger in magnitude than the forward current.

The obvious conclusion is that analytical response can be increased by using larger square wave amplitude, but, as in pulse voltammetry, increased amplitudes lead to broadening of the observed current peak. This effect is shown in Figure 4. The analytical choice must therefore be the largest value of square wave amplitude and step height consistent with adequate peak definition and evaluation. Of note in Figure 4 is the increase in the width of the current peak as the square wave amplitude becomes smaller than the step height.

The step height has little effect on the height of the current peak. For a square wave amplitude of 20 mV the peak current function $\Delta\psi_{max}^{+}$ goes from 0.642 for an $n\Delta E = 1$ mV to 0.686 for an $n\Delta E = 10$ mV ($\sigma = 5$, $\rho_1 = .499$, $\rho_2 = .999$). The individual forward and reverse currents, on the other hand, are markedly affected by the increase in step height. This is shown in Figure 5. The forward current function increases when the step height is increased but the reverse current function also increases, becoming less negative. The magnitude of change for both currents is approximately the same, so the difference current remains relatively unchanged.

Figure 5 is for constant τ, therefore the sweep rate is increasing as the step height is increased. It is interesting to note that increasing the sweep rate by increasing the step height has little effect on the difference

current function. Increasing the sweep rate by decreasing τ will cause the current to increase as $1/\sqrt{\tau}$ for a reversible system. If we compare two step heights at constant sweep rate, we find a marked difference in $\Delta\psi^+_{max}$. For example, given a sweep rate of 500 mV/sec that we can generate with a 10 mV step of 20 msec period or a 5 mV step of 10 msec period, the normalized peak current values $\Delta\psi^+_{max} (\tau)^{-1/2}$ for these are 4.85 and 6.64 respectively.

The important thing to remember is that the peak current will not only depend on the sweep rate but also on how that sweep rate is generated. Decreasing τ to obtain a faster sweep rate is better than increasing ΔE. The values of τ that can be used will, of course, depend on the system response.

The effect of measurement time is shown in Figure 6. These curves are calculated for a symmetric square wave ($\sigma=0.5$) and symmetric measurement times: $\rho_2 = \sigma+\rho_1$. As the measurement time is moved toward the beginning of the pulse, the difference current function greatly increases. As Ramaley and Krause have shown, the increase in peak current obtained by shortening the measurement time is greater than the increase obtained by keeping the measurement times at the end of the pulse and decreasing the staircase period. For the conditions of Figure 6, the peak value of the current function goes as $\rho_1^{-0.6}$ while the peak current depends on $\tau^{-0.5}$.

Some of the effects of asymmetric measurement on an asymmetric square wave are shown in Figure 7. The data for the bottom curve are calculated for variable σ with $\rho_1 = \sigma-0.001$ and ρ_2 fixed at 0.999. For these conditions, the peak current function is a minimum near $\sigma=0.5$ and increases essentially symmetrically on both sides of the minimum. The plot of the maximum values of $\Delta\psi^+$ vs σ becomes exactly symmetrical as the ratio $\Delta E/E_{sw}$ decreases.

Figure 8 details the individual forward and reverse current functions for three members of the set. For $\sigma = .1$ (Figure 8A) ψ_f is larger than $\Delta\psi^+$ because the reverse current function, ψ_r, has the same sign as ψ_f. This is

due to insufficient material being generated by the forward pulse to allow the reverse reaction to occur during the entire reverse pulse. As σ approaches τ, ψ_r gets more negative with a corresponding reduction in ψ_f until at $\sigma = 0.9$, the reverse pulse is not of sufficient length to regenerate the material consumed during the forward pulse. At this point ψ_f is at its lowest value while ψ_r is at a maximum (negatively). However, the change on ψ_r is greater than the decrease in ψ_f and thus the increase in $\Delta\psi^+$.

The data for the top curve of Figure 7 is again calculated for variable σ, this time with ρ_1 fixed at 0.049 and $\rho_2 = \sigma+0.049$. ρ_1 and ρ_2 are now positioned close to the switching points where ψ_f and ψ_r are maximum during their individual steps. The peak function $\Delta\psi^+$ is now a maximum at $\sigma = .5$, decreasing almost symmetrically on each side. Again the plot becomes exactly symmetrical at large square wave amplitude to step height ratios.

Individual forward and reverse currents for three members of this set are shown in Figure 9. The trends for the individual current function ψ_f and ψ_r are the same here as in Figure 8. ψ_f decreases and ψ_r increases (negatively) as σ approaches 0.9. However, in contrast to Figure 8 where the negative magnitude of ψ_r changes dramatically as σ goes from 0.1 to 0.9, the change in ψ_r here is relatively small.

Figure 10 illustrates the information that can be gained by a study of the individual forward and reverse current functions. This is a vertical comparison of two members in Figure 7. Here σ and ρ_1 are the same for both figures, equal to .1 and .099 respectively and ρ_2 is varied from close to the switching point (0.149) Fig.10A to near the end of the step (0.999) Fig. 10B. From examination of the reverse current function, it is obvious that the current during the reverse step has actually changed direction. Directly after the forward step ψ_r is opposite in sign to ψ_f while near the end of the step ψ_f and ψ_r has the same sign. This indicates that the material

generated by the forward pulse has been consumed during the first part of the reverse pulse and in order for the Nernst equation and Fick's laws of diffusion to be obeyed, the current near the end of the step must now flow in the same direction as ψ_f.

There is no obvious reason to output the difference current in which the current at ρ_1 during the jth cycle is differenced with the current at ρ_2 during the same staircase period. Since we have calculated and stored the partial current components, it is a simple matter to examine other differencing schemes, such as the backward difference, $\Delta\psi^-(j) = \psi_f(j) - \psi_r(j-1)$. This difference function has somewhat larger maximum values, especially at smaller square wave amplitudes, as can be inferred from an inspection of the potential dependence of the partial components shown in Figure 2. The apparent peak potential is shifted by approximately one-half the step height, relative to the maximum of the forward difference. Some representative and comparative values of the maximum peak current function ($\Delta\psi_{max}$), peak potentials and peak widths for forward and backward differences are shown in Table I.

The similarity of this technique to pulse polarography is obvious, although as has been demonstrated, variations in points of measurement affect the shape of the wave. Nevertheless, the equations developed result in wave shapes identical to those for differential pulse polarography (1) at slow scan rates and measurements parameters identical to those employed in pulse polarography.

Work is in progress to develop the theory to include the case of slow electron transfer processes, and first-order chemical processes, including preceeding, following and catalytic reactions.

Experimental verification of the theory presented here and demonstration of the analytical utility of the method at the dropping mercury electrode will be forthcoming (6).

CREDIT

TABLE I

| n E_{sw} mV | $W_{\frac{1}{2}}$, ψ^+ | | | | | $W_{\frac{1}{2}}$, ψ^- | | | | |
	Front Side mV	Back Side mV	Total Width mV	Peak Potential mV vs $E_{\frac{1}{2}}$	$\Delta\psi^+_{max}$	Front Side mV	Back Side mV	Total Width mV	Peak Potential mV vs $E_{\frac{1}{2}}$	$\Delta\psi^-_{max}$
5	45.9	46.7	92.6	-1.5	.1988	45.4	44.7	90.1	-1.8	.2158
10	46.3	46.8	93.1	- .95	.3609	46.2	45.7	91.9	-2.2	.3771
15	47.1	47.5	94.6	- .70	.5166	47.2	46.8	94.0	-2.5	.5315
20	48.3	48.7	97.0	- .58	.6636	48.5	48.2	96.7	-2.6	.6769
30	51.7	52.1	103.8	- .43	.9246	52.1	51.8	103.9	-2.7	.9340
40	56.4	56.7	113.1	- .33	1.137	57.0	56.6	113.6	-2.8	1.143
50	62.2	62.6	124.8	- .26	1.301	62.9	62.5	125.4	-2.9	1.304

Conditions: $n\Delta E = 5$ mV, $\sigma = .5$, $\rho_1 = 0.499$, $\rho_2 = 0.999$

LITERATURE CITED

1. J. G. Osteryoung, J. H. Christie, R. A. Osteryoung, Bull. Soc. Chim. Belg., 84, 647 (1975).

2. H. Blutstein and A. M. Bond, Anal. Chem., 48, 248 (1976).

3. G. C. Barker, Congr. on Anal. Chem. in Ind., St. Andrews, June, 1957.

4. L. Ramaley and M. S. Krause, Jr., Anal. Chem., 41, 1362 (1969).

5. M. S. Krause, Jr. and L. Ramaley, Anal. Chem., 41, 1365 (1969).

6. J. A. Turner, J. H. Christie, M. Vukovic and R. A. Osteryoung, to be submitted to Anal. Chem.

7. J. H. Christie and P. J. Lingane, J. Electroanal. Chem., 10, 176 (1965).

8. G. C. Barker, Anal. Chim. Acta, 18, 118 (1958).

9. T. Kambara, Bull. Chem. Soc. Japan, 27, 523 (1954).

10. S. C. Rifkin and D. H. Evans, Anal. Chem., 48, 1616 (1976).

FIGURE CAPTIONS

Figure 1.   Square wave waveform with associated nomenclature, τ is the step width for the base staircase.

Figure 2.   Individual and difference current functions for three square wave amplitudes. $n\Delta E = 5$ mV, $\sigma = 0.5$, $\rho_1 = 0.499$, $\rho_2 = 0.999$

(A) $nE_{sw} = 5$ mV

(B) $nE_{sw} = 15$ mV

(C) $nE_{sw} = 30$ mV

Solid line is difference current function, $\Delta\psi^+$

Figure 3.   Individual and difference current functions at the peak $(\Delta\psi^+_{max})$ vs square wave amplitude. $n\Delta E = 5$ mV, $\sigma = 0.5$, $\rho_1 = 0.499$, $\rho_2 = 0.999$.

($\blacksquare$) $\Delta\psi^+_{max}$

($\bullet$) ψ_f at peak

($\blacktriangle$) ψ_r at peak

Figure 4.   Peak width at half height vs square wave amplitude. $n\Delta E = 5$ mV, $\sigma = 0.5$, $\rho_1 = 0.499$, $\rho_2 = 0.999$.

Figure 5.   Individual forward and reverse current functions as a function of ΔE. $nE_{sw} = 20$ mV, $\sigma = 0.5$, $\rho_1 = .499$, $\rho_2 = .999$

(A) $n\Delta E = 10$ mV

(B) $n\Delta E = 5$ mV

(C) $n\Delta E = 2$ mV

(D) $n\Delta E = 1$ mV

Figure 6.   Effect of measurement time on $\Delta\psi^+$. $n\Delta E = 5$ mV, $nE_{sw} = 20$ mV, $\sigma = 0.5$, $\rho_2 = \sigma + \rho_1$

(A) $\rho_1 = .05$

(B) $\rho_1 = 0.1$

(C) $\rho_1 = 0.3$

(D) $\rho_1 = 0.499$

Figure 7.   Peak current function, $\Delta\psi_{max}^{+}$, vs σ. $n\Delta E = 5$ mV, $nE_{sw} = 20$ mV.

                ($\blacklozenge$) $\rho_1 = \sigma - 0.001$, $\rho_2 = 0.999$

                ($\blacktriangle$) $\rho_1 = 0.049$, $\rho_2 = \sigma + 0.049$

Figure 8.   Effect of asymmetric measurements on asymmetric square waves.

           $n\Delta E = 5$ mV, $nE_{sw} = 20$ mV, $\rho_1 = \sigma - .001$, $\rho_2 = .999$.

           (A) $\sigma = 0.1$

           (B) $\sigma = 0.5$

           (C) $\sigma = 0.9$

           Symmetry of waveform shown in inset, (x) indicates current

           measurement.

Figure 9.   Effect of asymmetric measurements on asymmetric square waves.

           $\rho_1 = 0.049$, $\rho_2 = \sigma + 0.049$, other conditions and legend same

           as Figure 8.

Figure 10.   Change in current function with sampling time $n\Delta E = 5$ mV,

           $nE_{sw} = 20$ mV, $\sigma = 0.1$, $\rho_1 = 0.099$
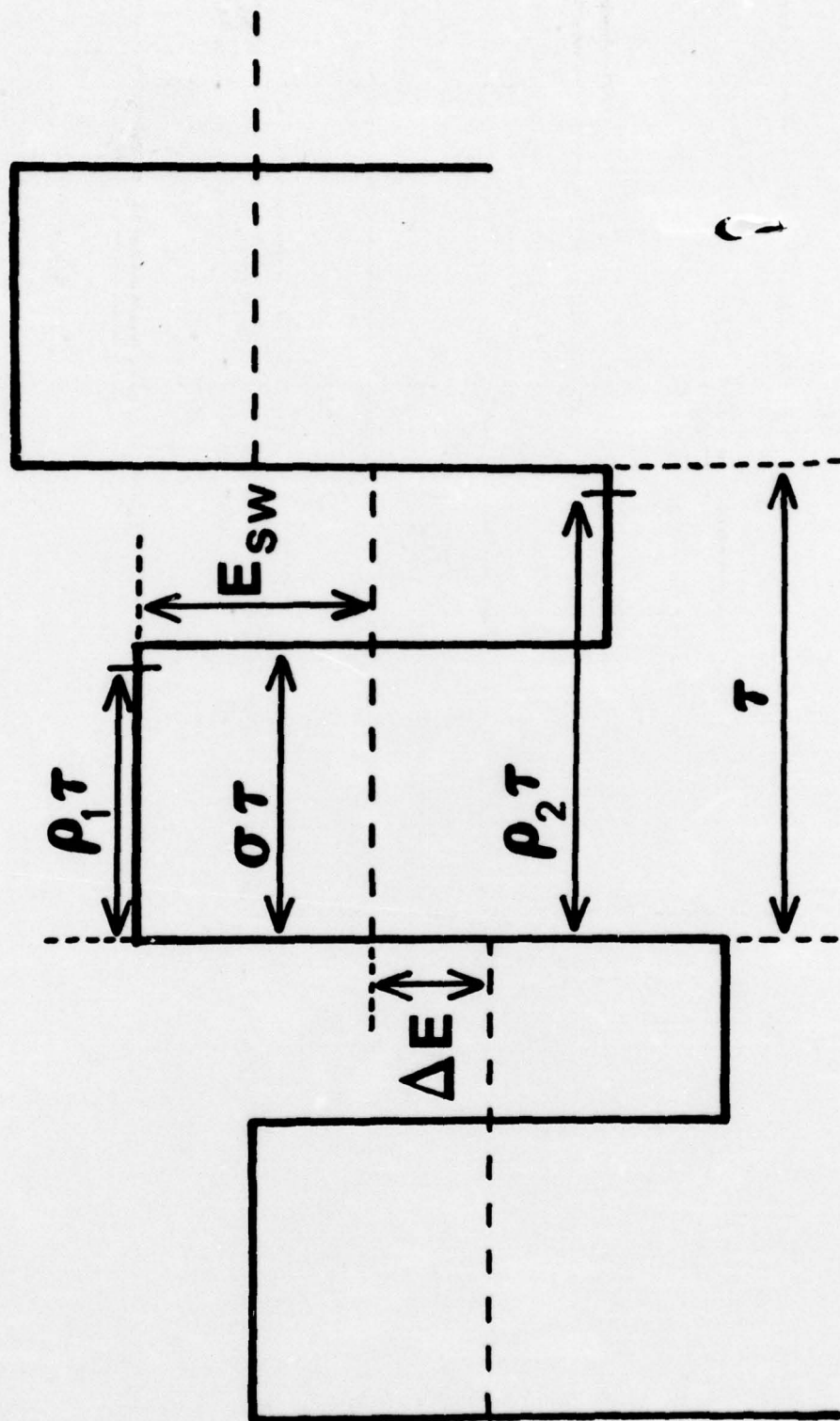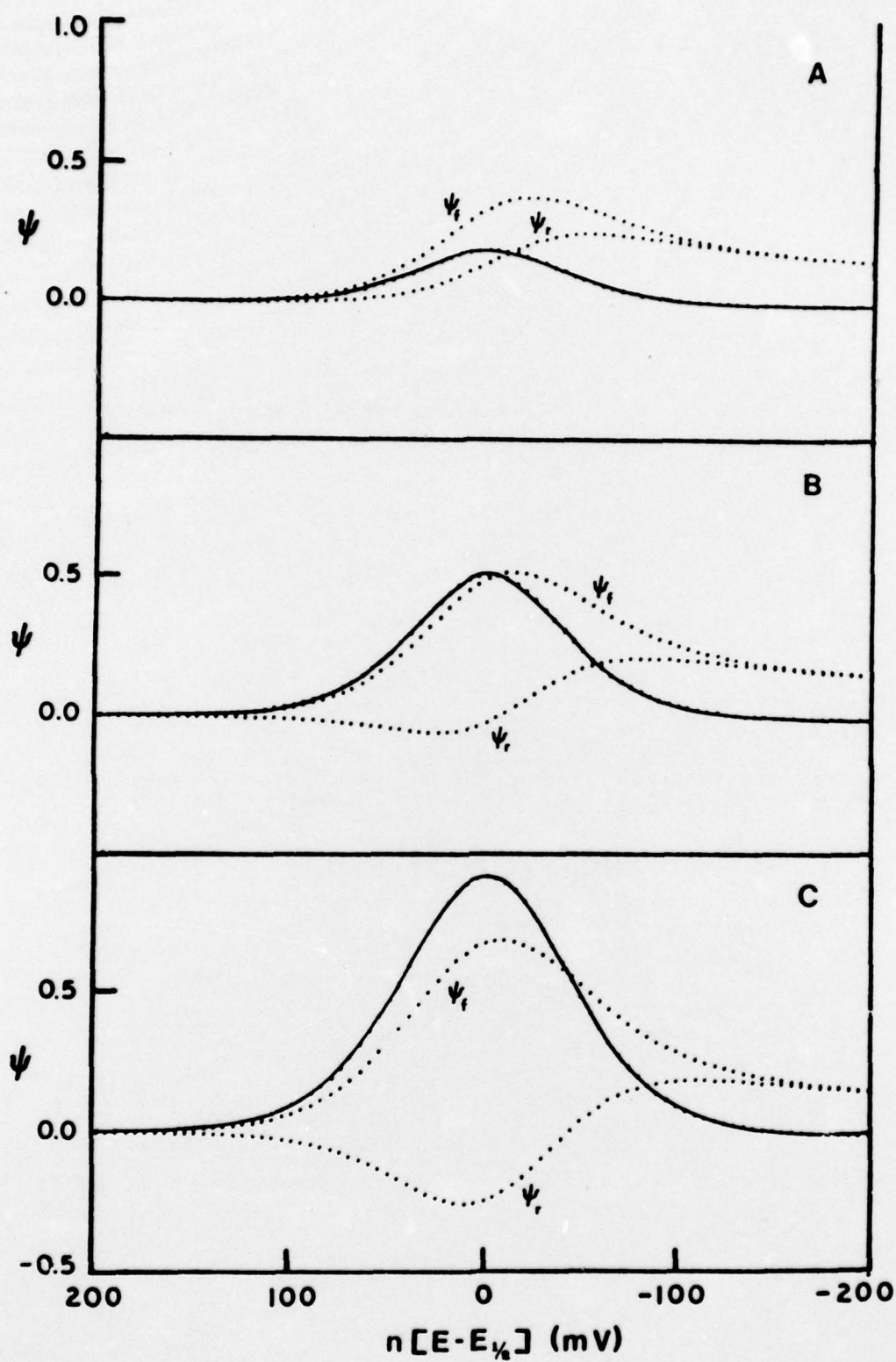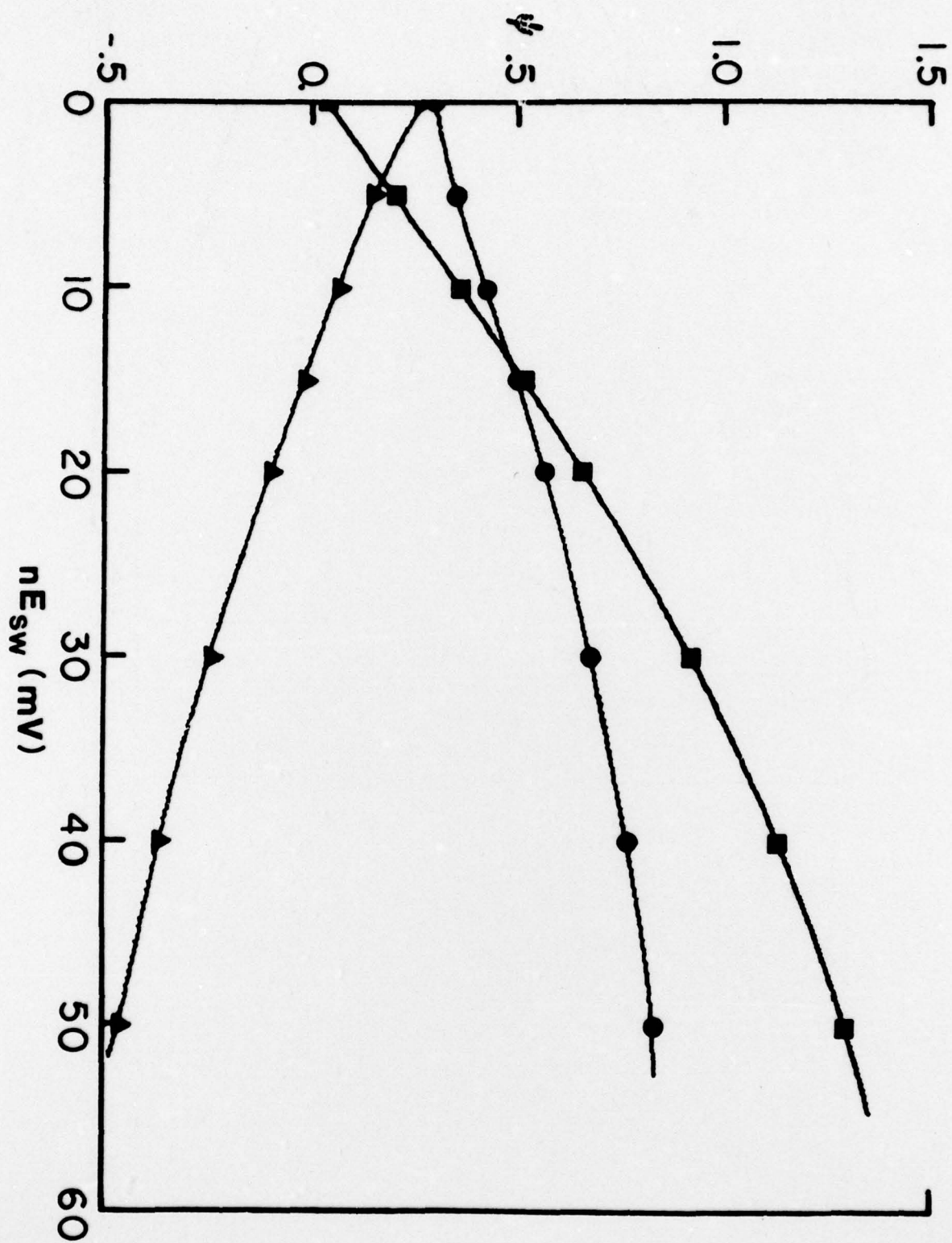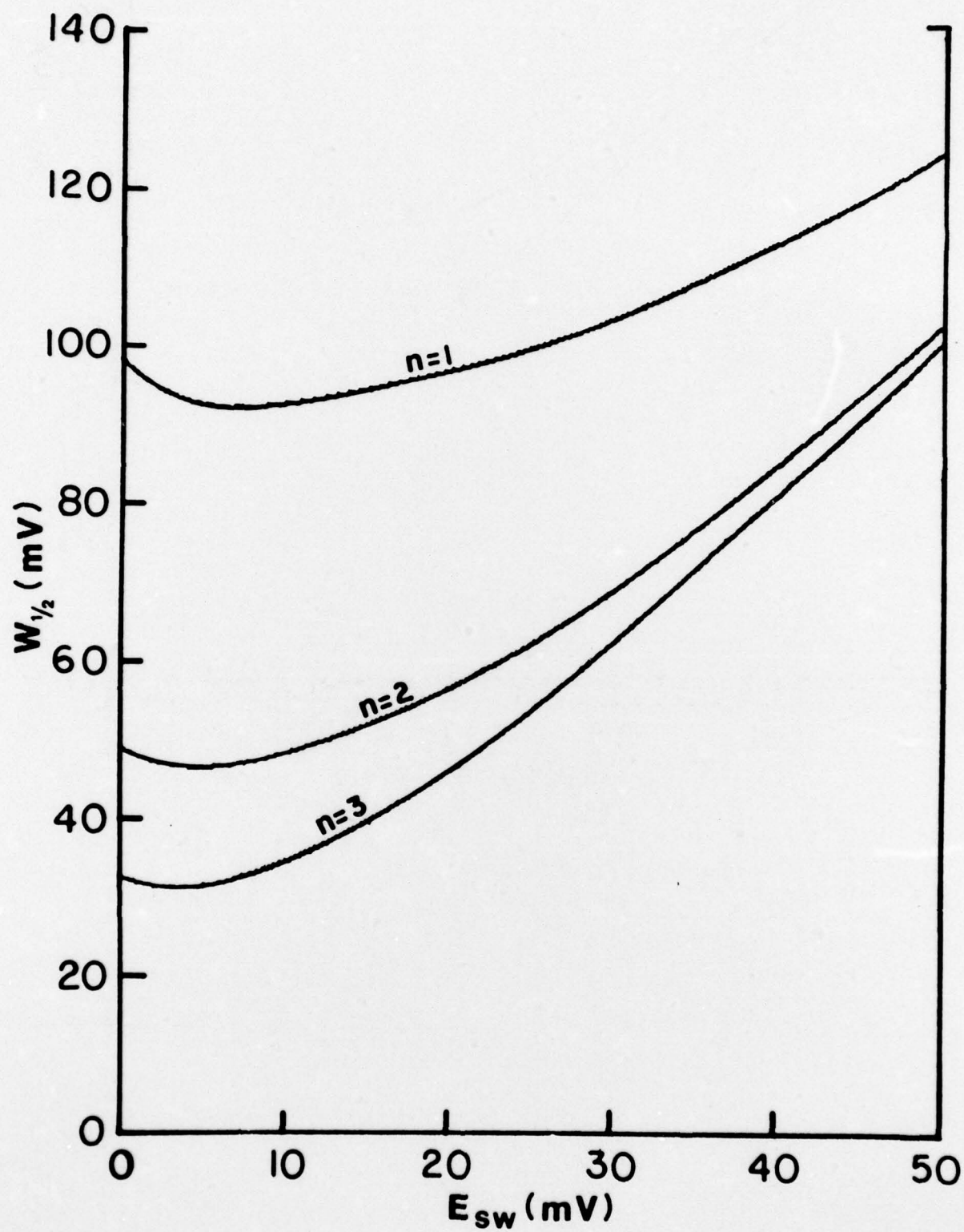
           (A) $\rho_2 = 0.149$
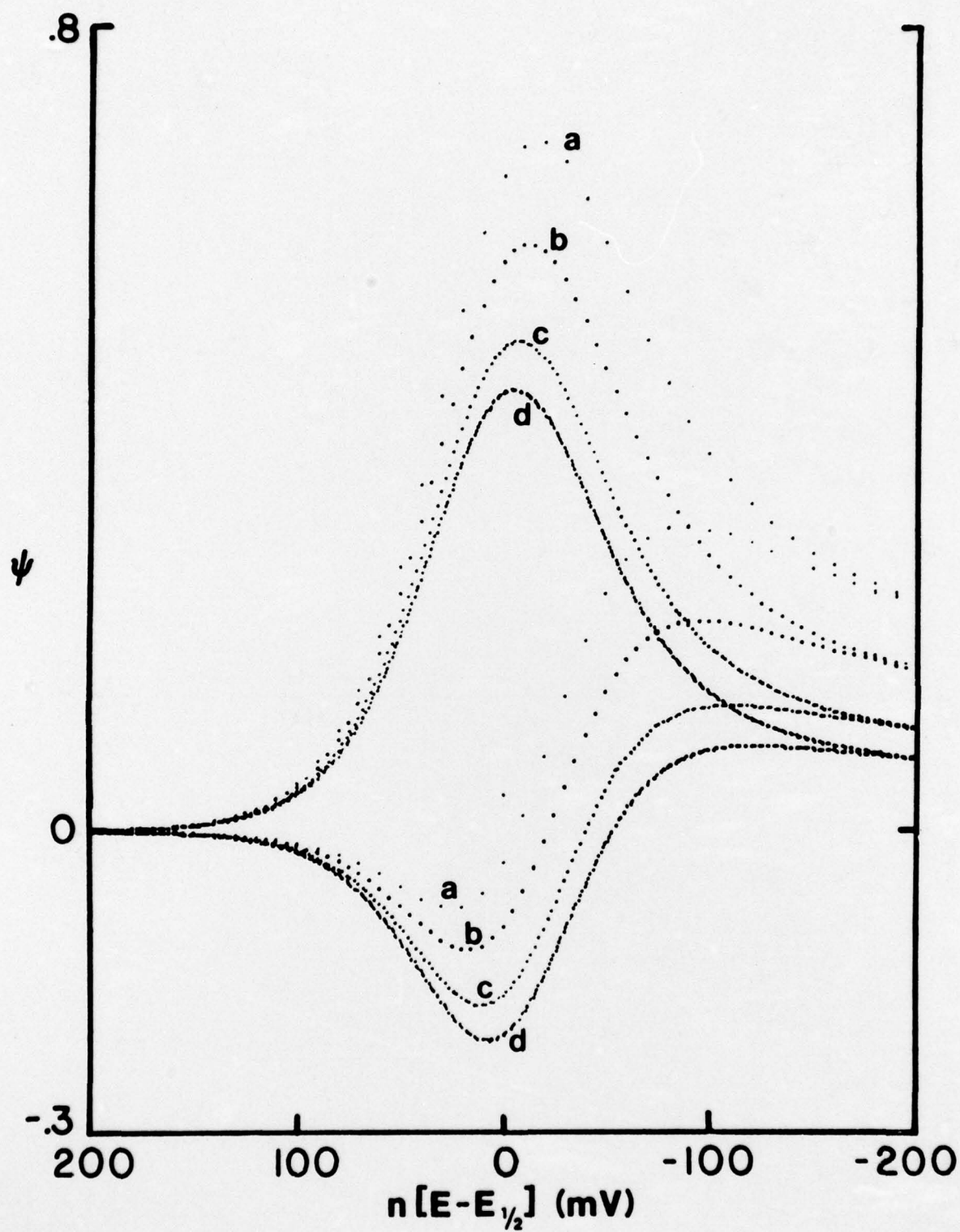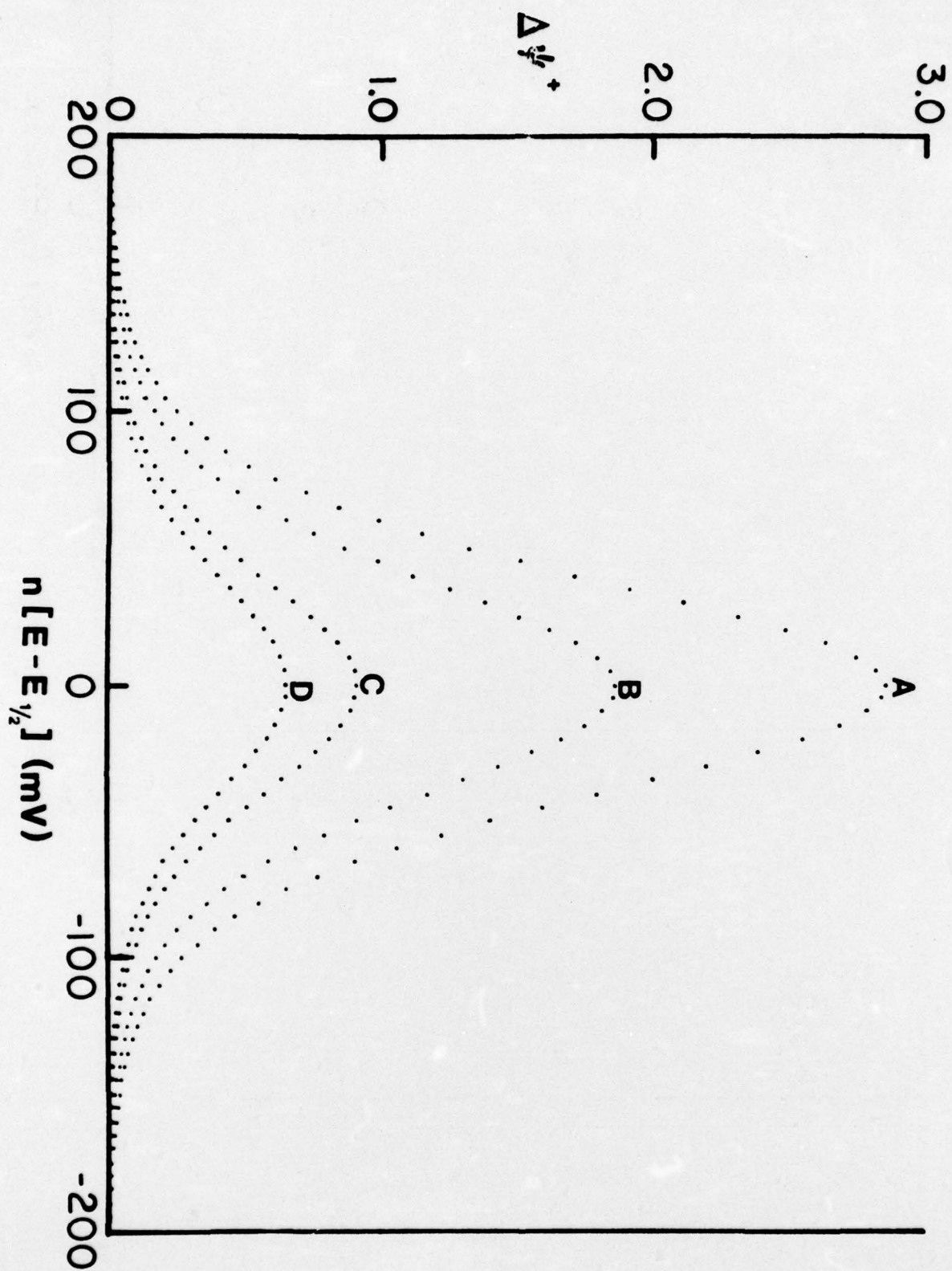
           (B) $\rho_2 = 0.999$

Figure 1

Figure 2

Figure 3

Figure 4

Figure 5

Figure 6
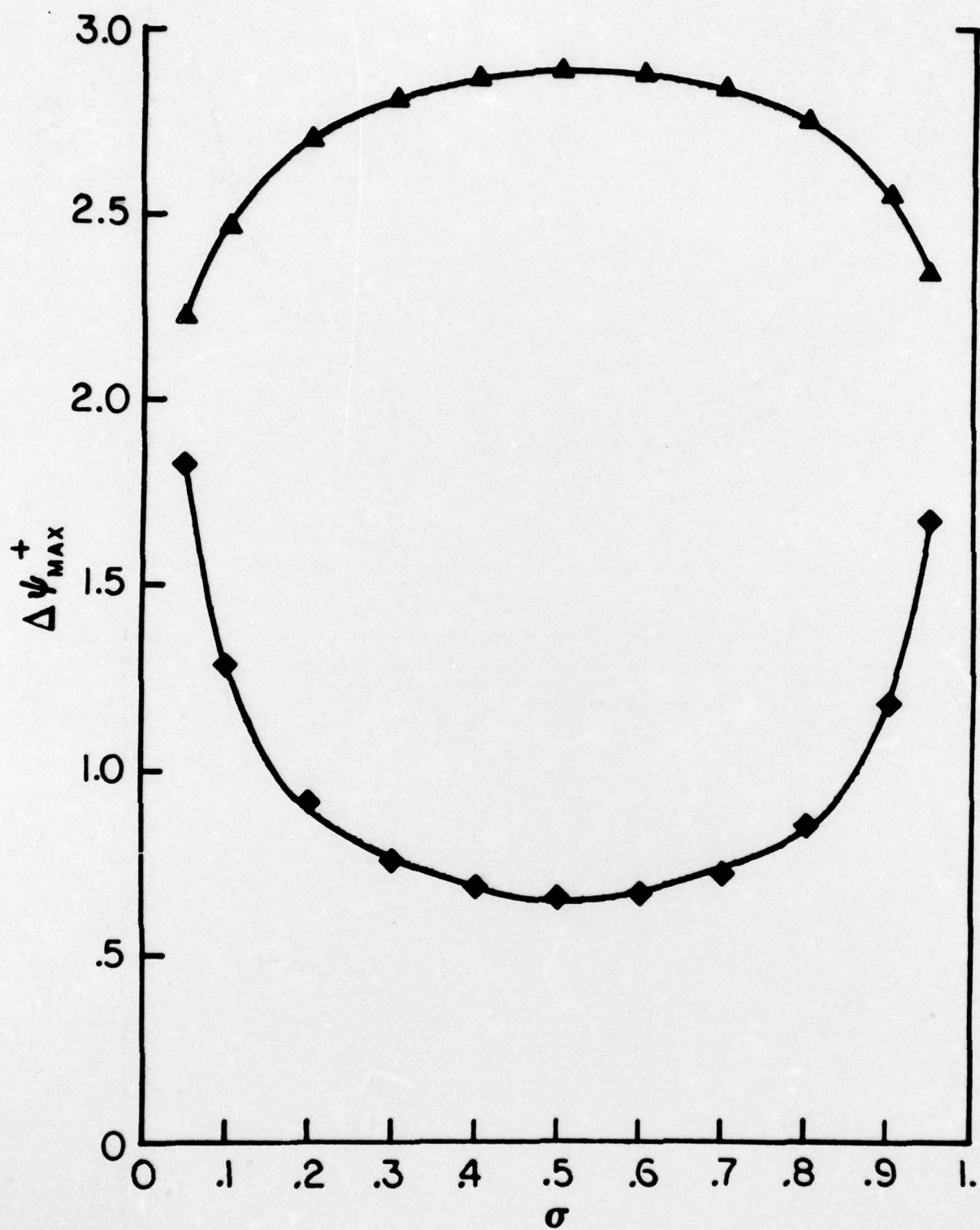
Figure 7
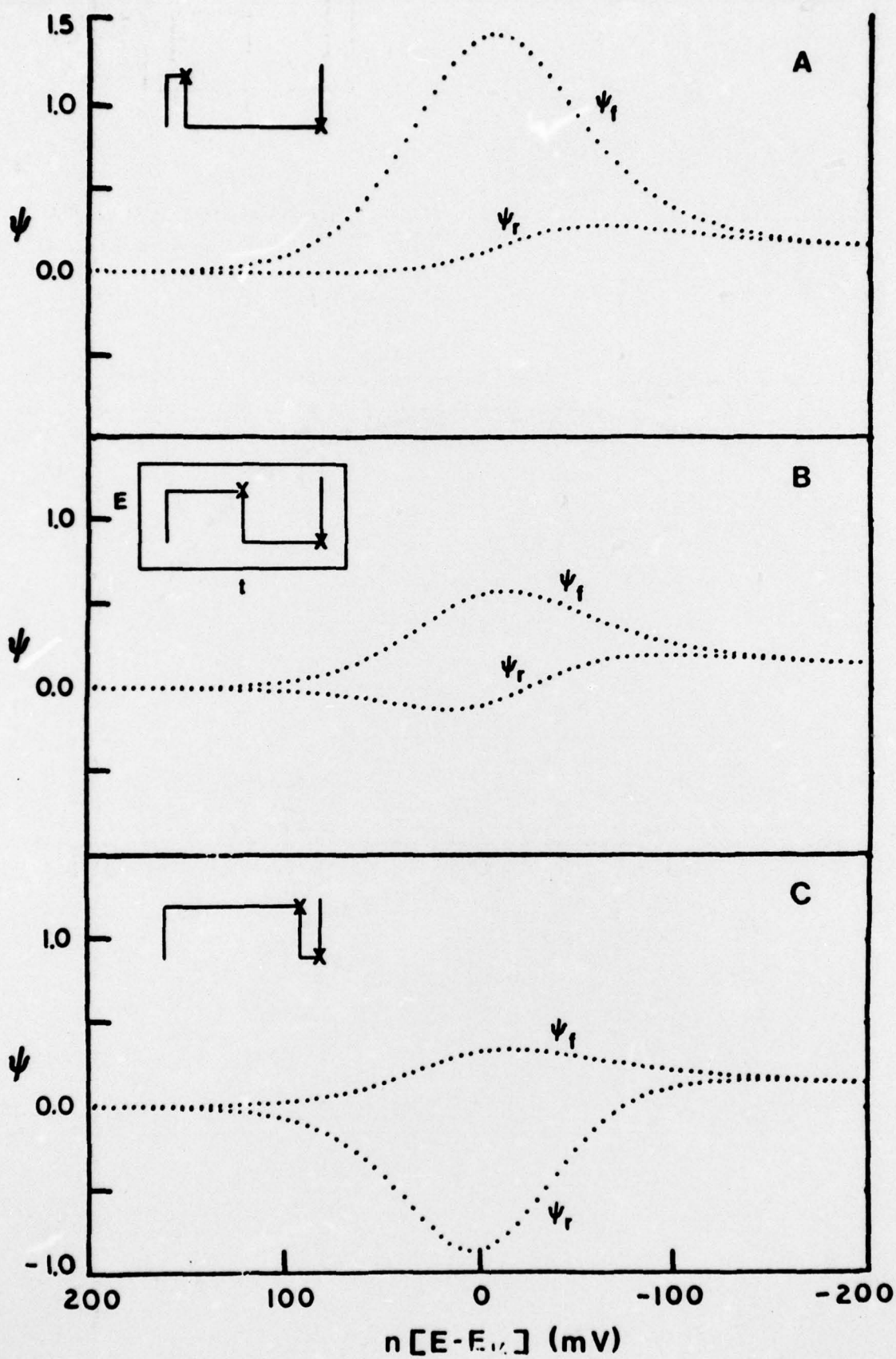
Figure 8
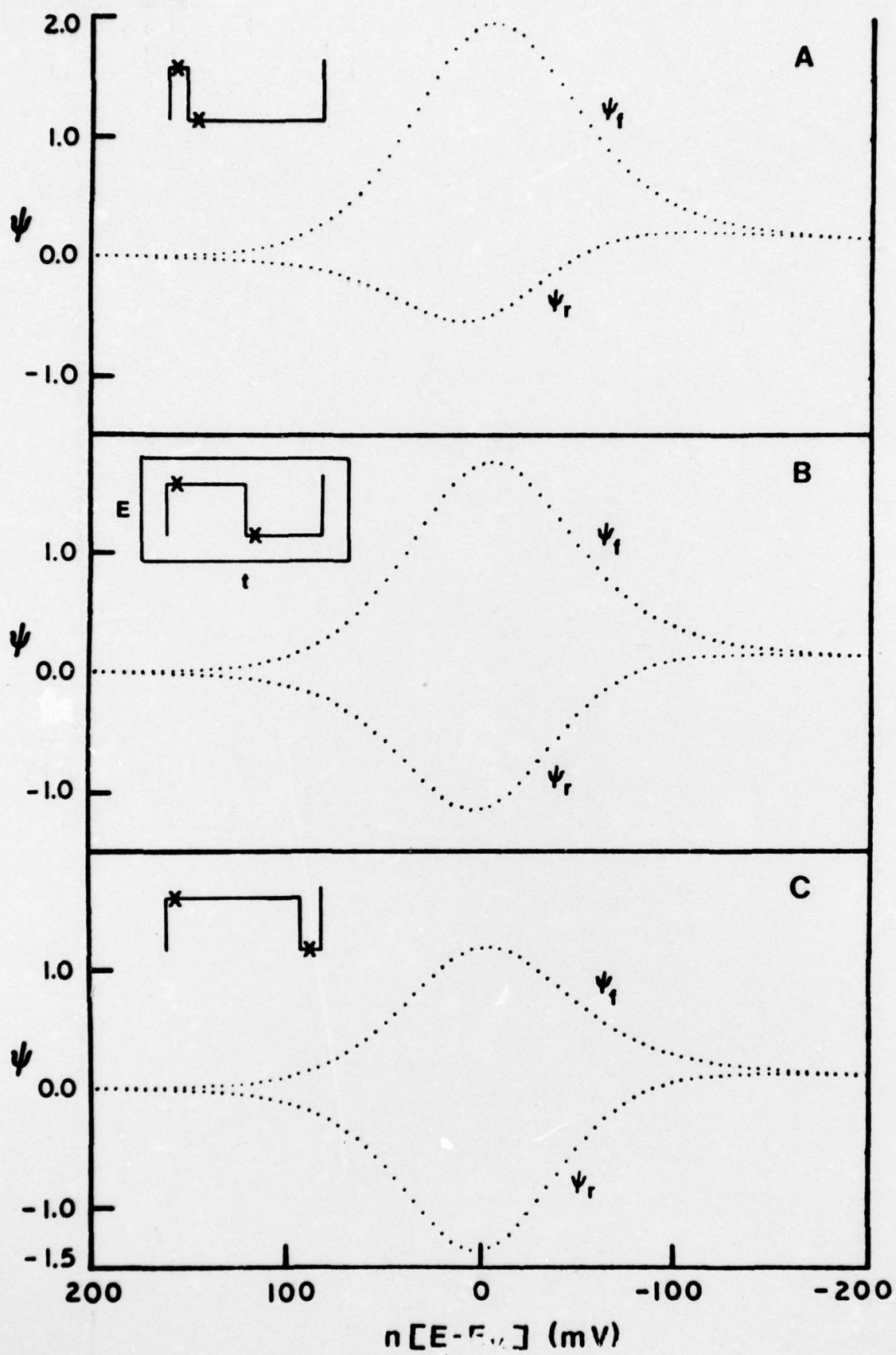
Figure 9
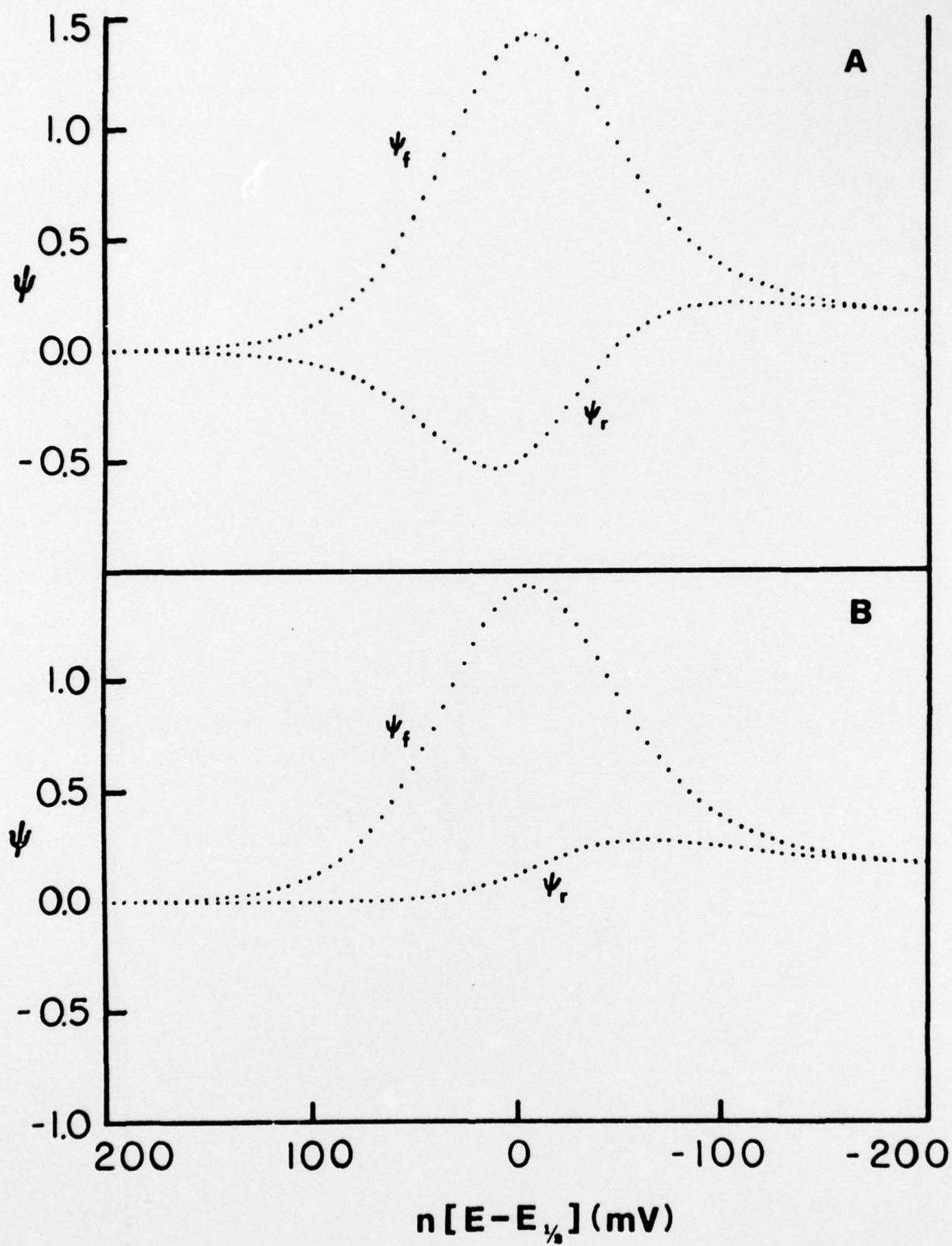
Figure 10

No. Copies   No. Co

Office of Naval Research Arlington, Virginia 22217 Attn: Code 472	2
Office of Naval Research Arlington, Virginia 22217 Attn: Code 102IP	6
ONR Branch Office 536 S. Clark Street Chicago, Illinois 60605 Attn: Dr. George Sandoz	1
ONR Branch Office 715 Broadway New York, New York 10003 Attn: Scientific Dept.	1
ONR Branch Office 1030 East Green Street Pasadena, California 91106 Attn: Dr. R. J. Marcus	1
ONR Branch Office 760 Market Street, Rm. 447 San Francisco, California 94102 Attn: Dr. P. A. Miller	1
ONR Branch Office 495 Summer Street Boston, Massachusetts 02210 Attn: Dr. L. H. Peebles	1

Director, Naval Research Laboratory
Washington, D.C. 20390
Attn: Library, Code 2029 (ONRL)   6
      Technical Info. Div.   1
      Code 6100, 6170   1

The Asst. Secretary of the Navy (R&D)
Department of the Navy
Room 4E736, Pentagon
Washington, D.C. 20350   1

Commander, Naval Air Systems Command
Department of the Navy
Washington, D.C. 20360
Attn: Code 310C (H. Rosenwasser)   1

Defense Documentation Center
Building 5, Cameron Station
Alexandria, Virginia 22314   12

U.S. Army Research Office
P.O. Box 12211
Research Triangle Park, North Carolina 277
Attn: CRD-AA-IP

Commander
Naval Undersea Research & Development
Center
San Diego, California 92132
Attn: Technical Library, Code 133   1

Naval Weapons Center
China Lake, California 93555
Attn: Head, Chemistry Division   1

Naval Civil Engineering Laboratory
Port Hueneme, California 93041
Attn: Mr. W. S. Haynes   1

Professor O. Heinz
Department of Physics & Chemistry
Naval Postgraduate School
Monterey, California 93940

Dr. A. L. Slafkosky
Scientific Advisor
Commandant of the Marine Corps (Code RD-1)
Washington, D.C. 20380   1

No. Copies   No. Co]

Dr. Paul Delahay
New York University
Department of Chemistry
New York, New York 10003   1

~~Dr. R. A. Osteryoung~~
~~Colorado State University~~
~~Department of Chemistry~~
~~Fort Collins, Colorado 80521~~   ~~1~~

Dr. E. Yeager
Case Western Reserve University
Department of Chemistry
Cleveland, Ohio 41106   1

Dr. D. N. Bennion
University of California
Energy Kinetics Department
Los Angeles, California 90024   1

Dr. J. W. Kauffman
Northwestern University
Department of Materials Science
Evanston, Illinois 60201   1

Dr. R. A. Marcus
University of Illinois
Department of Chemistry
Urbana, Illinois 61801   1

Dr. M. Eisenberg
Electrochimica Corporation
2485 Charleston Road
Mountain View, California 94040   1

Dr. J. J. Auborn
GTE Laboratories, Inc.
40 Sylvan Road
Waltham, Massachusetts 02154   1

Dr. Adam Heller
Bell Telephone Laboratories
Murray Hill, New Jersey   1

Dr. T. Katan
Lockheed Missiles & Space Co., Inc.
P.O. Box 504
Sunnyvale, California 94088   1

Dr. R. A. Huggins
Stanford University
Department of Materials Science
    & Engineering
Stanford, California 94305

Dr. Joseph Singer, Code 302-1
NASA-Lewis
21000 Brookpark Road
Cleveland, Ohio 44135

Dr. B. Brummer
EIC Incorporated
55 Chapel Street
Newton, Massachusetts   02158

Library
P. R. Mallory and Company, Inc.
P. O. Box 706
Indianapolis, Indiana 46206

Dr. P. J. Hendra
University of Southampton
Department of Chemistry
Southampton SO9 5NH
United Kingdom

Dr. Sam Perone
Purdue University
Department of Chemistry
West Lafayette, Indiana 47907

Dr. Royce W. Murray
University of North Carolina
Department of Chemistry
Chapel Hill, North Carolina 27514

Dr. J. Proud
GTE Laboratories Inc.
Waltham Research Center
40 Sylvan Road
Waltham, Massachusetts 02154

Mr. J. F. McCartney
Naval Undersea Center
Sensor and Information Technology Dep
San Diego, California 92132

No. Copies   No. Copies

Dr. J. H. Ambrus   Dr. D. L. Warburton
The Electrochemistry Branch   The Electrochemistry Branch
Materials Division, Research & Technology Dept.   Materials Division, Research & Technol
Naval Surface Weapons Center   Dept.
White Oak Laboratory   Naval Surface Weapons Center
Silver Spring, Maryland 20910   1   White Oak Laboratory
                                                          Silver Spring, Maryland 20910   1
Dr. G. Goodman
Globe-Union Inc.   Dr. R.C. Chudacek
5757 North Green Bay Avenue   McGraw-Edison Company
Milwaukee, Wisconsin 53201   1   Edison Battery Division
                                                          Post Office Box 28
Dr. J. Boechler   Bloomfield, New Jersey 07003   1
Electrochimica Corporation
Attention: Technical Library
2485 Charleston Road
Mountain View, California 94040 1